We thank the Reviewer #1 for evaluating our paper, both here, and at the technical level. The reviewer's comments, and our replies/revisions, are in red and black, respectively.

Page 26594

line 15: change 'in' to 'on'

Author's Change to Manuscript: Second, we use our measurement to derive a temperature- and aerosol-dependent fit of $N_{IC}$ based on Eq. (1).

line 24: 'heterogeneous ice generation can be distinguished …' : Please be more specific in how they can be distinguished

Author's Change to Manuscript: The foundations of our investigation are the cold-season middle-tropospheric wave cloud studies of Cooper and Vali (1981), Cotton and Field (2002), Eidhammer et al. (2010) and Field et al. (2012). The prior research demonstrated that an assessment of wave cloud kinematics can be used to distinguish heterogeneous nucleation from homogeneous ice nucleation and that crystal production occurs primarily via the previously-mentioned freezing nucleation pathways. Further, no compelling evidence for secondary ice production was reported in those prior studies.

Page 26596

line 25 ff.: to readers who are not familiar with FSSP, PCASP and 2DC measurements it might not be clear from the description that evaporation is intended or may be a problem of the instrument. Please be more explicit here.

Author's Response: We feel that the manuscript makes it clear that evaporation, due to heating of the sample stream, is an issue for measurements made with the PCASP (haze particles and cloud droplets), but not for measurements made with the FSSP (cloud droplets) or with the 2DC (ice crystals). Further, we used the words "evaporate" and "evaporation" in our description of the PCASP measurement (bottom of p. 26596). Finally, we also stated that the PCASP measurements used to evaluate $n_{0.5}$ were acquired outside of cloud (Sections 3.3 and 3.4) where neither our work (Snider and Petters, 2006), or the work of Strapp et al. (1992), reveals a "problem of the instrument." To emphasize this point, we modified the sentence on Page 26602, Line 11.

Author's Change to Manuscript: These were averaged outside of cloud during the five-second time windows used for thermodynamic-property averaging (Sect. 3.1).

Page 26600

line 7: ‘This is shown, for the example,..’: delete ‘the’

Author’s Change to Manuscript: An example of this is shown in Fig. 1d.

Page 26602

line 6: Please describe more explicit the effect you observe of ice nucleation on cloud properties which is evident in Figure 1.

Author’s Change to Manuscript: The effect of ice development on cloud properties is evident at the downwind track-streamline intersection in Figs. 1 and 2. Most noticeable are the enhanced lidar depolarization ratios seen at $x \geq 15$ km in Fig. 1c and the enhanced diameter-integrated crystal concentrations seen at $x \geq 15$ km in Fig. 2d.

Page 26604

line 7: A short description of D10's three-step procedure would help the reader to follow the method described in this manuscript.

L5-L6, P26604 was modified to this:

Author's Change to Manuscript: ...using the three-step procedure described in D10. We refer to the latter as method #2 and describe our implementation of that method in Appendix B (attached below).

Page 26605

line 4 ff.: Is the fraction of the measured crystal concentrations that plot within a factor of two of the fit still significantly different if the error of the measured ice crystal concentrations is taken into account?

Author's Response: In the table shown below, we evaluate the effect of the Poisson sampling error on the fractions. Regardless of how the comparison is made the conclusion is the same: More points plot within a factor-of-two when using Eq. (1) with our Method #1 coefficients.

**Fraction of $N_{IC}$ Measurements within a Factor of two of the Fit**

| | Eq. (1) with Method #1 Fit Coefficients | Eq. (1) with D10 Fit Coefficients |
|---|---|---|
| Manuscript L. 4 / P. 26605 | 0.69 | 0.66 |
| Measurements Increased by Poisson Sampling Error | 0.74 | 0.72 |
| Measurements Decreased by Poisson Sampling Error | 0.65 | 0.52 |

Page 26606

line 11 ff.: Is should be stressed more that already the original D10 equation fits well to the measured data. This is of high value because of the very different measurement methods.

Author's Change to Manuscript: The result we present in Tab. 2, with fit coefficients generally consistent, in a statistical sense, with those reported by D10, is important because it validates D10's approach using different methodology.

Page 26606

line 20: insert 'ice' before 'nuclei'

Author's Change to Manuscript: We also probed the conjecture that the duration of ice nuclei exposure to water-saturated conditions is a determinant of IC concentration.

**References**


Cooper, W.A., and G. Vali, The origin of ice in mountain cap clouds, J. Atmos. Sci., 38, 1244-1259, 1981

Cotton, R. and P. Field, Ice nucleation characteristics of an isolated wave cloud, Q. J. Roy. Meteor. Soc., 128, 2417-2437, 2002

DeMott, P.J., A.J. Prenni, X. Liu, S.M. Kreidenweis, M.D. Petters, C.H. Twohy, M.S. Richardson, T. Eidhammer and D.C. Rogers, Predicting global atmospheric ice nuclei distributions and their impacts on climate, P. Natl. Acad. Sci., 107, 11217-11222, 2010

Eidhammer, T., P. J. DeMott, A. J. Prenni, M. D. Petters, C. H. Twohy, D. C. Rogers, J. Stith, A. Heymsfield, Z. Wang, K. A. Pratt, K. A. Prather, S. M. Murphy, J. H. Seinfeld, R. Subramanian, and S. M. Kreidenweis, Ice initiation by aerosol particles: Measured and predicted ice nuclei concentrations versus measured ice crystal concentrations in an orographic wave cloud, J. Atmos. Sci., 67, 2417-2436, 2010

Field, P.R., A.J. Heymsfield, B.J. Shipway, P.J. DeMott, K.A. Pratt, D.C. Rogers, J. Stith and K.A. Prather, Ice in clouds experiment-layer clouds. Part II: Testing characteristics of heterogeneous ice formation in lee wave clouds, J. Atmos. Sci., 69, 1066-1079, 2012

Snider, J.R., and M.D. Petters , Optical particle counter measurement of marine aerosol hygroscopic growth, Atmos. Chem. Phys., 8, 1949-1962, 2008

Strapp, J.W., W.R. Leaitch and P.S.K. Liu, Hydrated and dried aerosol-size-distribution measurements from the particle measuring systems FSSP-300 probe and the deiced PCASP-100x Probe, J. Atmos. Oceanic Tech., 9, 548-555, 1992

## Appendix B

Here we describe how we fitted our 80 measurements of the set $\{N_{IC}, n_{0.5}, T_{low}\}$ using the three step procedure developed by D10 (herein method #2). In the first step, the data were binned into four $(273.16 - T_{low})$ subsets; the number of samples in the four subsets is provided in Table 3. In the second step, values of $ln(p_i)$ and $q_i$ were derived for each subset by regression. Here "$i$" indicates the temperature subset and the form of the fitted equation is

$$ln(N_{IN,i}) = ln(p_i) + q_i \cdot ln(n_{0.5,i}) \quad \text{(B1)}$$

In the third step, the values of $ln(p_i)$ were regressed vs. $ln(273.16 - T_{low,i})$, and also, the values of $q_i$ were regressed vs. $T_{low,i}$. In these regressions the $T_{low,i}$ is the average of the subset. The slopes and intercepts of these regressions define the coefficients $ln(a)$, $b$, $c$ and $d$ for method #2.

$$ln(a) = \text{intercept}\left(ln(p_i)\ vs.\ ln(273.16 - T_{low,i})\right) \quad \text{(B2)}$$

$$b = \text{slope}\left(ln(p_i)\ vs.\ ln(273.16 - T_{low,i})\right) \quad \text{(B3)}$$

$$c = \text{slope}\left(q_i\ vs.\ (273.16 - T_{low,i})\right) \quad \text{(B4)}$$

$$d = \text{intercept}\left(q_i\ vs.\ (273.16 - T_{low,i})\right) \quad \text{(B5)}$$

We thank the Reviewer #2 for evaluating our paper. The reviewer's comments, and our replies/revisions, are in red and black, respectively.

The paper combines parcel modelling of streamlines through wave clouds with observations from aircraft to test the DeMott et al. 2010 ice nucleation parameterization. The authors also attempt to investigate the importance of time dependent freezing.

The paper is well written and concise and potentially a good test of a commonly used ice nuclei representation. However, the determination of ice concentration from 50 micron size particles, that is used to directly compare to the DeMott et al. formula is my biggest concern. Measurements of these particle sizes is highly uncertain and this problem needs to be addressed more thoroughly before this paper can be published.

Major points:

26597:13-26598:20

The determination of ice concentration from 50 micron size particles is my biggest concern. This needs to be addressed before this paper can be published.

Shattering has been discounted, but it would be easy to quickly assess the fraction of particles with unusually short interarrival times to support the authors assumption.

Author's Response: We provide an analysis of interarrival time in Appendix A (attached). That analysis backs up what we say in the paper on P26597L20. Also, after L24, we added text telling the reader that further analysis of the 2DC measurements is provided in Appendix A.

Author's Addition to Manuscript: Crystal concentration and crystal interarrival time measurements, derived using the 2DC, are analyzed in greater detail in Appendix A.

The authors quote a comparison made between oil coated slides and the 2DC as proof of the reliability of using that measurement. At best that comparison is only valid for the 2dc probe with the configuration of electronics, optics and processing used at the time. I think that the later paper by Strapp et al. (2001, J. Atmos. Ocean. Technol.,18, 1150–1170) is more general and supersedes those previous findings.

Author's Response:

We talked with Perry Wechsler, our engineer. His technical records indicate that with the exception of the addition of RAM, to replace shift registers and routine maintenance including laser replacement, the probe's optical and mechanical characteristics are the same as in Cooper and Saunders (1980). However, data recording and processing of the raw data has changed and neither was implemented, in our work, as in Cooper and Saunders (1980).

An analysis of measurements, made in 2011, with the Wyoming 2DC and our CIP probe, purchased in 2009, is described in Appendix A (attached). That result is consistent with the findings of Cooper and Saunders (1980).

Strapp et al. 2001 note that variation in time response and thresholds for the 2DC probes mean that sizing for particles smaller than 125 micrometers is highly uncertain. That uncertainty in sizing affects the assumed depth of field and translates into large uncertainties and biases in the concentration. Corrections have been proposed (references in Strapp et al.), but knowledge of the response characteristics, depth of field and detection threshold is required.

Author's Response:

A comparison of 2DC- and CIP-derived concentrations is provided in Appendix A (attached). We demonstrate reasonable agreement among 2DC-derived and CIP-derived concentrations for crystals greater than 50 um. Our finding (Appendix A) runs contrary to the expectation that the faster responding CIP should report concentrations larger than the slower responding 2DC (Baumgardner et al., 2001). We conclude that the 2DC concentrations (D>50um) are not as strongly biased as suspected by the reviewer.

Baumgardner, D., H.Jonsson, W.Dawson, D.O'Connor and R.Newton, The cloud, aerosol and precipitation spectrometer: a new instrument for cloud investigations, Atmos. Res., 59-60, 251-264, 2001

Possible solutions are to use a larger ice size threshold for which the concentrations are more reliable combined with an estimate of the number concentration of ice crystals larger than that threshold.

Author's Response: We don't agree with the approach suggested by the reviewer. The CIP/2DC comparison (Appendix A) supports our contention that the 2DC-derived concentrations (D>50um) are sufficient for comparing ice in clouds to the prediction of the D10 parameterization. Also, indirect support can be found in Heymsfield et al. (2013; their Appendix A), who compared CIP-derived and 2DS-derived concentrations (D>50um) and report good agreement.

Heymsfield, A.J., C.Schmitt, and A.Bansemer, Ice cloud particle size distributions and pressure-dependent terminal velocities from in situ observations at temperatures from 0° to −86°C, J. Atmos. Sci., 70, 4123–4154, 2013

26605:10 Mixedphase time. I like what the authors have attempted to do, but the 5K temperature ranges are large. From DeMott et al 2010, the change in ice concentration would need to be greater than a factor of 2 in order to be observed for a 5K temperature window. I think that the authors need to add this to their discussion about what they are able to say about the importance of time dependent ice nucleation.

Author's Response: We missed this point and have modified the text accordingly:

Author's Change to Manuscript: As was discussed in the introduction, there is an outstanding question in atmospheric science community regarding the time-dependent nature of ice nucleation. Of relevance for our data set, with its average $t_{MP}$ =221 s (Sect. 3.2), is the possibility that the characteristic time for a subcritical ice embryo to transition to a detectable ice particle is comparable to $t_{MP}$. If that were the case, we would expect that streamlines associated with larger mixed-phase times, all other things equal, would have larger IC concentrations. The work of Vali and Snider (2014) provides an estimate the effect. They show that time dependency can alter crystal concentrations by up to a factor of three depending on whether stochastic or singular theory is used to describe nucleation.

Author's Change to Manuscript (start of paragraph): We investigated time dependency by stratifying our 80 determinations of $\{N_{IC}, n_{0.5}, T_{low}, t_{MP}\}$ into four $T_{low}$ subsets.

Added Reference: Vali, G. and Snider, J. R., Time-dependent freezing rate parcel model, Atmos. Chem. Phys. Discuss., 14, 29305-29329, doi:10.5194/acpd-14-29305-2014, 2014

Author's Response: Related to this, we changed the following paragraph:

Author's Change to Manuscript: In spite of these suggestions of a connection between crystal concentration and mixed-phase time we cannot argue convincingly that time-dependent effects were significant for crystals within the clouds we studied. Our ability to

argue for, or against a dependence on $t_{MP}$, was limited by the strong temperature-dependence of ice nucleation. This is evident from Fig. 3a where the value $k_2 = 0.22\ ^oC^{-1}$ can be used to demonstrate that a 5 $^o$C decrease corresponds to a factor of three increase in nucleated concentration. Also limiting is the relatively few data values within our 5 $^o$C subsets. Thus, in future wave cloud studies, attention should be paid to strategies which generate an adequate number of points within specified temperature and aerosol ranges.

Minor points:

26593:5. By 'latter' do you mean heterogeneous freezing?

Author's Response: We removed the sentence.

26601:10. At this point in the text I don't understand why the relative value was computed.

Author's Response: The relative value is used later in the paper (P26605L23) to discard points associated large mixed-phase time uncertainty.

26602:24. Condition 1) indicates that N(D>25micrometers) has to be greater than 2xN(D<50micrometers) for inclusion.

Author's Response: We strived to make this statement consistent with what we said in Section 2.2. We revised this to improve clarity:

Author's Change to Manuscript: (1) $N_{IC}$(D<50μm) must be smaller than $0.5 \cdot N_{IC}$(D>25μm) (Sect. 2.2),

## Appendix A

In this appendix we examine the reliability of ice crystal concentrations derived using the University of Wyoming 2DC. We derive concentrations using the Wyoming 2DC, with its slower-responding photodiode array (Gayet et al., 1993; Baumgardner and Korolev, 1997; Strapp et al., 2001), and compare to values derived using a faster responding cloud imaging probe (CIP; Baumgardner et al., 2001). We also analyze the 2DC ice crystal interarrival times and investigate crystal shattering. Two data sets are analyzed. The first comes from Wyoming King Air flight data, acquired on 9 January 2011 during the Colorado Airborne Multi-Phase Cloud Study (CAMPS), and the second comes from the 80 downwind track-streamline intersections described in Sect. 3.5. Both the 2DC and CIP were operated with standard probe tips (Korolev et al., 2013).

Strapp et al. (2001) conducted laboratory studies that investigated a 2DC's ability to detect objects (circular dots) positioned away from the center of focus of the probe's laser. They demonstrated that the probe's finite response led to undersizing, counting losses and image distortion. At dot sizes smaller than 100 μm, undersizing and counting losses increased with the speed the dots transited through the probe's sample volume. Strapp et al. conducted their testing using dots deposited onto a glass disk. The dots were opaque, monodisperse, and regularly spaced on the disk along circular tracks. The disk was positioned with its rotational axis parallel to the 2DC laser beam. The position of the disk plane, relative to the center of focus of the beam, was varied. The largest dot speeds tested by Strapp et al. were comparable to the airspeed of the Wyoming King Air (~100 m/s).

### A1 - 2DC and CIP Concentrations

A comparison of 2DC- and CIP-derived concentrations was made using Wyoming King Air data acquired on 9 January, 2011 (20110109). The comparison data was selected from three

level-flight transits of an orographic cloud. The cloud was located over continental divide in northern Colorado. During the cloud transits the liquid water content was less than 0.2 g $m^{-3}$ and temperature was between -23 and -25 $^{o}$C. We processed the raw 2DC and CIP measurements the same way we processed the WAICO 2DC measurements (Sect. 2.2). Also consistent with the WAICO processing, the compared concentrations are five-second averages and are for crystals larger than 50 μm (sized along the aircraft track). The CIP/2DC comparison is shown in Fig. A1a. The vertical line at 5 $L^{-1}$ marks the median of the 80 concentrations in our WAICO data set (Sect. 3.5), and its implication is discussed in the following paragraph.

Because of the undersizing and counting losses documented for a 2DC, especially at the low end of its range (D < 100 μm), and the fact these effects are attributed to the relatively slow time response of the 2DC's optical array (Strapp et al., 2001), it is expected that concentrations derived using the faster responding CIP (Baumgardner et al., 2001) should exceed 2DC-derived values. Contrary to that expectation, we found reasonable agreement (Fig. A1a). Measures of the agreement are as follows: 1) For concentrations larger than 5 $sL^{-1}$, all of the 2DC-derived values plot well within a factor of two of the CIP. 2) For concentrations smaller than 5 $sL^{-1}$, a large fraction of the 2DC values (87%) plot within a factor of two of the CIP. These findings, combined with the findings of Cooper and Saunders (1980) (also see Sect. 2.2), lend confidence to the concentration values we derived using 2DC measurements made during WAICO. However, this comparison does not completely lessen the concern that we biased the WAICO concentrations at D < 100 μm by assuming that the 2DC's optical depth of field was independent of crystal size and equal to the probes's sampling aperture (61 mm) (Vali et al., 1981 and Sect. 2.2).

**A2 - Interarrival Time and Shattering**

316 Representative CIP and 2DC size distributions, from CAMPS, are shown in Fig. A1b. It is
317 evident that most of the detected crystals are smaller than 400 μm, especially in the 2DC
318 measurement. A size distribution from one of the 80 WAICO downwind track-streamline
319 intersections is shown in Fig. A2a. The largest crystal detected in this five-second interval is 400
320 μm. A histogram of crystal interarrival times for the same five-second interval is shown in Fig.
321 A2b. Evident in the left tail of the histogram is a minimum, at interarrival time $\tau^*$ = 2x10$^{-3}$ s,
322 where we delineate between a fragment mode ($t < \tau^*$) and a mode corresponding to intact
323 crystals ($t > \tau^*$). We note that 7% of the crystal counts classify as fragments and that this
324 fraction is much smaller than the example presented by Korolev et al. (2013) for a 2DC with
325 standard probe tips (their Fig. 14a).

326 We analyzed interarrival times obtained from each of the 80 WAICO downwind track-
327 streamline intersections. Histograms were binned as in A2b (3.5 bins per decade) and all particle
328 images, including those that did not pass the rejection criteria of Pokharel and Vali (2011) (Sect.
329 2.2), were used. We developed a procedure that searches the histogram for a minimum
330 between $t$ = 10$^{-6}$ s and the histogram mode. In our set of 80 there are 16 cases that do not
331 exhibit a minimum and 21 with a provisionally significant minimum. The provisional cases were
332 characterized by a cumulative fraction, evaluated at the minimum, greater than 20%. The
333 example shown in Fig. A2b is not a provisional case because the cumulative fraction at $\tau^*$ =
334 2x10$^{-3}$ s is less than 20%. All of the provisional cases exhibited a minimum that was within an
335 order of magnitude of the histogram mode. Because order-of-magnitude separation is
336 substantially less than the minimum-to-mode separation seen Korolev et al. (2013) (their Fig.
337 14), we concluded that a fragment mode could not be discerned. Thus, we ignored the effect of
338 shattering. Twenty six of the remaining 43 cases (43=80-16-21) had a minimum more than an

339 order of magnitude smaller than the histogram mode; Fig. A2b is an example. For these we
340 ignored the effect of shattering because the fraction affected was less than 20% and because
341 the rejection criteria of Pokharel and Vali (2011) removes some of the affected crystals from the
342 population used to evaluate the concentration.

343

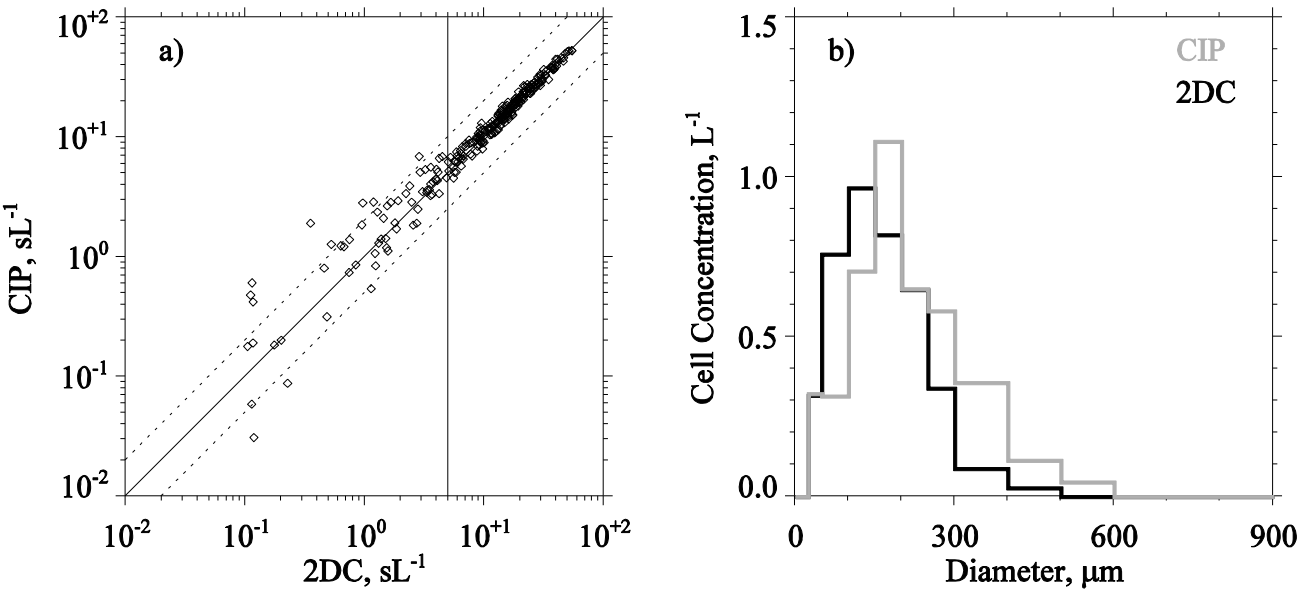


Fig. A1 – a) The CIP/2DC concentration comparison. Compared values are five-second averages and are for crystals larger than 50 µm. Comparison data is from 20110109 during the Colorado Airborne Multi-Phase Cloud Study (CAMPS). Wyoming King Air data shown here was selected from three along-wind level-flight cloud transits: 1) 221200 to 222200 UTC, 2) 223900 to 224800 UTC, and 3) 230600 to 231600 UTC. The vertical line at 5 $sL^{-1}$ is drawn at the median value for our set of 80 WAICO 2DC-derived measurements. b) 2DC and CIP size distributions from a representative five-second subset (224646 to 224650 UTC) of the CAMPS cloud transits on 20110109.

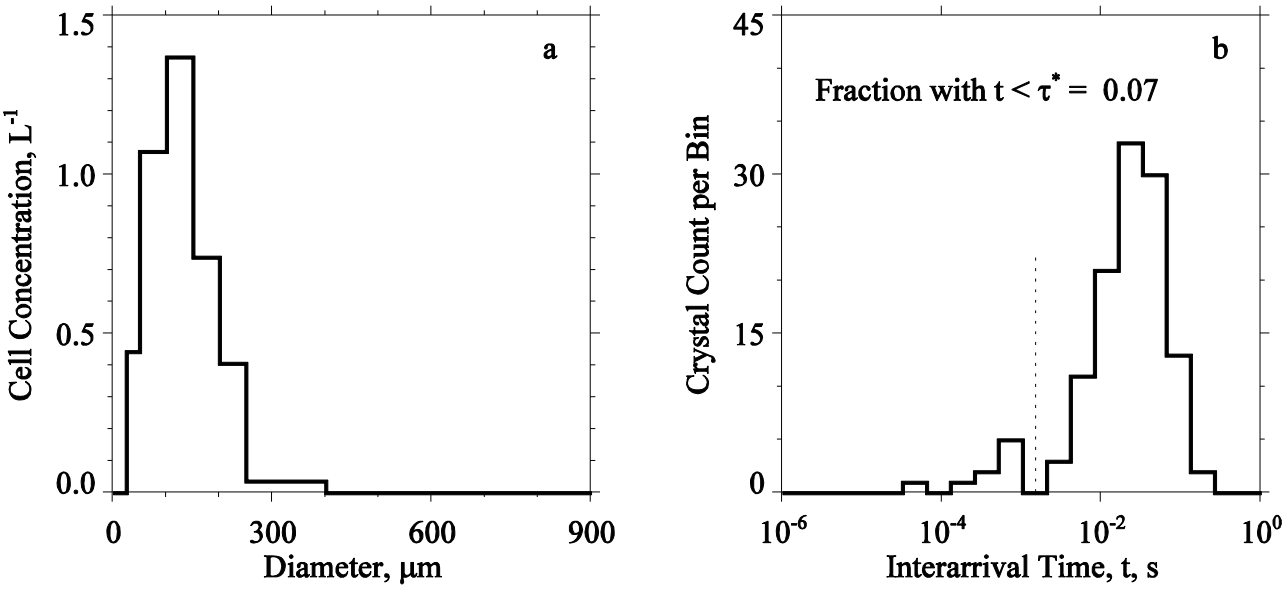


Fig. A2 – a) The 2DC size distribution derived for the WAICO 181933 to 181937 interval on 20080227. This interval corresponds to the downwind track-streamline intersection at x=15 km in Fig. 1c. b) The interarrival time histogram for the 181933 to 181937 interval on 20080227. The vertical dashed line marks a minimum between a fragment mode ($t < \tau^*$) and a mode corresponding to intact crystals ($t > \tau^*$).

## References


Baumgardner, D., H.Jonsson, W.Dawson, D.O'Connor and R.Newton, The cloud, aerosol and precipitation spectrometer: a new instrument for cloud investigations, Atmos. Res., 59-60, 251-264, 2001

Baumgardner, D., and A.Korolev, Airspeed corrections for optical array probe sample volumes, J. Atmos. Oceanic Technol., 14, 1224-1229, 1997

Gayet, J.F., P.R.A. Brown, and F.Albers, A Comparison of In-Cloud Measurements Obtained with Six PMS 2D-C Probes. J. Atmos. Oceanic Technol., 10, 180–194, 1993

Korolev, A.V., E. F. Emery, J. W. Strapp, S. G. Cober, and G. A. Isaac, Quantification of the effects of shattering on airborne ice particle measurements, J. Atmos. Oceanic Technol., 30, 2527–2553, 2013

Strapp, J.W., F.Albers, A.Reuter, A.V.Korolev, U.Maixner, E.Rashke and Z.Vukovic, Laboratory measurements of the response of a PMS OAP-2DC, J. Atmos. Oceanic Tech., 18, 1150-1170, 2001

Atmos. Chem. Phys. Discuss., 14, 26591–26618, 2014
www.atmos-chem-phys-discuss.net/14/26591/2014/
doi:10.5194/acpd-14-26591-2014


Atmospheric Chemistry and Physics Discussions



# Ice crystal concentrations in wave clouds: dependencies on temperature, $D > 0.5\,\mu m$ aerosol particle concentration and duration of cloud processing

**L. Peng, J. R. Snider, and Z. Wang**

Department of Atmospheric Sciences, University of Wyoming, Laramie, WY, USA

Received: 26 July 2014 – Accepted: 18 September 2014 – Published: 23 October 2014

Correspondence to: J. R. Snider (jsnider@uwyo.edu)

Published by Copernicus Publications on behalf of the European Geosciences Union.







## Abstract

Model equations used to either diagnose or prognose the concentration of heterogeneously nucleated ice crystals depend on combinations of cloud temperature, aerosol properties, and elapsed time of supersaturated-vapor or supercooled-liquid conditions. The validity of these equations is questioned. For example, there is concern that practical limitations on aerosol particle time-of-exposure to supercooled-liquid conditions, within ice nucleus counters, can bias model equations that have been constrained by ice nuclei (IN) measurements. In response to this concern, this work analyzes airborne measurements of crystals made within the downwind glaciated portions of middle-tropospheric wave clouds. A streamline model is used to connect a measurement of aerosol concentration, made upwind of a cloud, to a downwind ice crystal (IC) concentration. Four parameters were derived for 80 streamlines: (1) minimum cloud temperature along the streamline, (2) aerosol particle concentration (diameter, $D > 0.5\,\mu m$) measured within ascending air, upwind of the cloud, (3) IC concentration measured in descending air downwind, and (4) the duration of water-saturated conditions along the streamline. The latter are between 38 to 507 s and the minimum temperatures are between −34 to −14 °C. Values of minimum temperature, $D > 0.5\,\mu m$ aerosol concentration and IC concentration were fitted using the equation developed for IN by DeMott et al. (2010; D10). Overall, there is reasonable agreement among measured IC concentrations, IN concentrations derived using D10's fit equation, and IC concentrations derived by fitting the wave cloud measurements with the equation developed by D10.

## 1 Introduction

Ice nucleation is a pivotal process in the evolution of many cloud types (Braham and Squires, 1974; Cantrell and Heymsfield, 2005; DeMott et al., 2010; Murray et al., 2012). Ice crystals form via different pathways; the two fundamental distinctions are homogeneous and heterogeneous nucleation. Temperatures colder than −35 °C, and the





ACPD
14, 26591–26618, 2014



existence of either haze particles or cloud droplets, are necessary conditions for the occurrence of the homogeneous pathway (Heymsfield and Miloshevich, 1993). Heterogeneous ice nucleation takes place on aerosol particles (ice nuclei, IN) and the known pathways are deposition, condensation freezing, immersion freezing and contact freezing (Vali, 1985; Murray et al., 2012). ~~This work is focused on the latter processes.~~

Two contrasting approaches are used to translate measurements into equations used to predict IN activation, and thus ice crystal (IC) concentration, in cloud models. The first of these is diagnostic in the sense that IC concentration is formulated solely in terms of thermodynamic and aerosol state properties. The second is state and time dependent. In model intercomparison studies (Eidhammer et al., 2009; Niemand et al., 2012), these two frameworks produce significantly different IC concentrations. There are many reasons for these inconsistencies; fundamentally, they result because the time scale characterizing the development of a subcritical ice embryo into an ice crystal (Bigg, 1953; Vali and Stansbury, 1966), and how properties of an aerosol particle influences embryo development, are inadequately understood (Murray et al., 2012; Vali, 2014). Another relevant factor, but one which attenuates the framework-to-framework differences (Eidhammer et al., 2009), is that the Bergeron–Findeisen process can act to slow, or even shut down, the freezing nucleation pathways (i.e., condensation, immersion and contact freezing).

Our primary focus is the temperature- and aerosol-dependent IN fit equation developed by DeMott et al. (2010; hereafter D10). The D10 equation, hereafter Eq. (1), was developed with measurements of activated IN concentration derived using the continuous flow diffusion chamber (CFDC; Rogers et al., 2001). The IN measurements were made concurrently with measurements of the concentration of aerosol particles with diameter ($D$) larger than 0.5 µm ($n_{0.5}$)

$$N_{\mathrm{IN}}(T, n_{0.5}) = a \cdot (T_{\mathrm{o}} - T)^{b} \cdot (n_{0.5})^{c\cdot(T_{\mathrm{o}}-T)+d} \quad (1)$$

Here $T$ is the temperature in the section of the CFDC operated above water saturation, $T_{\mathrm{o}}$ is a reference temperature (273.16 K), and $a, b, c$ and $d$ are the fitted coef-





ACPD
14, 26591–26618, 2014



ficients. We reexamine Eq. (1) because it was developed with the CFDC operating in a manner which restricted the upper-limit diameter of aerosol particles processed within the CFDC ($D < 1.6\,\mu m$) and which restricted the duration of the particle's exposure to water-saturated conditions ($t < 10\,s$). Since both of these restrictions can cause the IN concentration to be underestimated (D10; Wright et al., 2013; DeMott et al., 2014), we use measurements made in and near clouds to evaluate the potential bias.

We have three specific objectives. First we use our airborne measurements of IC concentration to derive a temperature-dependent fit of those measurements. We refer to these two properties as $N_{IC}$ and $N_{IC}(T)$, respectively. Specifically, we analyze IC concentration measurements recorded within the downwind (descending flow) portion of middle-tropospheric wave clouds, where IC concentration is thought to reflect IN activation that occurred upwind, within the colder and liquid-water saturated portion of the cloud. ~~Second, we use our measurements to derive a temperature- and aerosol-dependent fit of $N_{IC}$ based in Eq. (1).~~ We refer to the latter as $N_{IC}(T, n_{0.5})$. Third, we analyze our measurements of $N_{IC}$ with estimates of the interval of time an air parcel was exposed to water-saturation within a wave cloud. This is relevant to cloud modeling because many models employ a state- and time-dependent framework to predict IC concentration (e.g., Hoose et al., 2010). The IN, aerosol and IC concentrations relevant to our work are summarized in Table 1.

~~The foundations of our investigation are the wave cloud studies of Cooper and Vali (1981), Cotton and Field (2002), Eidhammer et al. (2010) and Field et al. (2012). Relevant to our work, these prior studies demonstrated that heterogeneous ice generation can be distinguished from both homogeneous nucleation, and from secondary ice production processes, and that the contribution from the deposition pathway is generally small in comparison to crystal production via the previously-mentioned freezing nucleation pathways.~~

Our investigation is most similar to the airborne studies of Eidhammer et al. (2010) and Field et al. (2012). Those authors analyzed cold-season (late fall) measurements





ACPD
14, 26591–26618, 2014



made near, and within, middle-tropospheric wave clouds during the ICE-L project conducted in 2007. Their measurements were made over northern Colorado and southern Wyoming. Similar to that work, we sampled wave clouds along horizontal flight legs and also made no attempt to use the aircraft to follow the wave streamlines. Our airborne measurements were made in 2008 and 2009, in the same region as the ICE-L study, and also during the cold season (late winter and early spring). We analyze measurements made at locations where a streamline model indicated our aircraft intersected air that ascended into, and descended from, wave clouds. As we will discuss in detail, we develop a data set from eight flights; 80 wave cloud streamlines are analyzed. In contrast, Eidhammer et al. (2010) analyzed data from one flight, and modeled three streamlines. Field et al. (2012) expanded that analysis, and reported on measurement/model comparisons for 28 streamlines. In their analyses, both Eidhammer et al. (2010) and Field et al. (2012) exercised a streamline-following aerosol and cloud microphysical parcel model, and both derived the model's initial thermal state using measurements made downwind of the investigated wave clouds. In contrast, we use a streamline model to track the thermodynamic and time-distance evolution of air parcels (parcel microphysics is not evaluated), and we use measurements made immediately upwind of the investigated clouds, within ascending air, to initialize the model.

## 2 Measurements

We analyze airborne remote sensing and airborne in-situ measurements from the Wyoming Airborne Integrated Cloud Observation (WAICO) study conducted 2008 and 2009 (Wang et al., 2012). All measurements were acquired onboard the University of Wyoming King Air. The base of operations was Laramie, Wyoming. All of the sampled clouds were in the altitude range 3700 to 7400 m, and were located north of Laramie, within 110 km.





ACPD
14, 26591–26618, 2014



## 2.1 Temperature and humidity

Temperature ($T$) was measured using a reverse-flow immersion thermometer (Lawson and Cooper, 1990). Dew point temperature ($T_{dp}$) was derived from vapor density measurements made with a LI-COR gas analyzer (model LI6262). The latter is characterized by a 0.2 s time response (Dobosy et al., 1997) and this value is somewhat smaller than the time response of the reverse-flow temperature sensor (~ 1 s; Rodi and Spyers-Duran, 1972). The inlet to the LI-COR was forward-facing and was operated subisokinetically with its inlet airspeed set at approximately 18 m s$^{-1}$. The latter is a factor of six smaller than the airspeed of the King Air (110 m s$^{-1}$).

## 2.2 Microphysics

Three wing-mounted optical particle counters are used in this analysis: (1) the Passive Cavity Aerosol Spectrometer Probe (PCASP), (2) the Forward Scattering Spectrometer Probe (FSSP), and (3) the Two Dimensional Optical Array Probe (2DC). Each of these was fabricated by Particle Measuring Systems (PMS; Boulder, CO).

The PCASP was used to measure the concentration of particles with diameters between 0.12 to 3.2 µm. Particle sizing was based on laboratory calibrations conducted using monodisperse test particles with refractive index $n = 1.59$ (Cai et al., 2013). PCASP concentrations were derived as the ratio of particle count rate divided by a calibrated sample flow rate (Cai et al., 2013).

Adiabatic compression warms the aerosol stream as it approaches the PCASP inlet. Strapp et al. (1992) estimated that this process occurs over 0.2 s. Once the stream reaches the probe, it is warmed by three anti-ice heaters (Snider et al., 2014). The time scale for diabatic (anti-ice) heating is approximately an order of magnitude smaller than the 0.2 s adiabatic warming. Because of both the adiabatic and diabatic processes, unactivated cloud droplets (haze particles), and cloud droplets, are partially evaporated prior to sizing within the PCASP. In the case of haze particles, evaporation is complete





ACPD
14, 26591–26618, 2014



if the initial particle diameter is smaller than ∼1 µm (Strapp et al., 1992; Snider and Petters, 2008).

The FSSP was used to categorize cloud droplets sizes from 1.5 to 47.5 µm into 15 bins. During WAICO the cloud droplet concentrations were less than 300 $cm^{-3}$, so the FSSP dead time and coincidence errors are less than 25 % (Baumgardner et al., 1985). Both of these effects were accounted for in the data processing. Because our FSSP measurements come from clouds containing ice, bias due to ice crystal shatter also needs to be addressed. Since we only analyze FSSP measurements recorded near the upwind edge of the clouds, where the ice crystals are small (< 100 µm) and their concentration is low (< 0.4 $L^{-1}$), the effect of shatter on the FSSP measurements is not expected to be significant (Gardiner and Hallett, 1985; Gayet et al., 1996; Field et al., 2003) and was not evaluated.

Ice crystals were sized and counted using an optical array probe (2DC) (Pokharel and Vali, 2011). This instrument records a crystal as a two-dimensional image. Some images were rejected using criteria described in Pokharel and Vali (2011). Images which passed the rejection tests were sized in the along-track direction (hereafter, this dimension is termed "diameter") and these were binned into channels with lower-limit diameters set at 25, 50, 100, 150, 200, 250, 300, and 400 µm for the smallest eight of 20 channels; nearly all crystals recorded during WAICO classified into these eight channels. Because even the largest crystals in this set are smaller than the size known to shatter when impacted at aircraft velocities (Korolev and Isaac, 2005; Korolev et al., 2013), the effect of shatter was ignored. Concentrations were derived with the assumption that the optical depth of field was independent of crystal size and equal to the 2DC's sampling aperture (61 mm) (Vali et al., 1981).

2DC-derived concentrations were validated by Cooper and Saunders (1980). The basis for their validation was airborne 2DC concentrations measured simultaneous with concentrations derived by impacting ice crystals onto oil-coated slides (OCS) exposed in a decelerator. Crystals impacted on the slides were photographed and counted, the counts were increased by dividing by a size-dependent impaction efficiency, and





ACPD
14, 26591–26618, 2014



diameter-integrated concentrations were computed for crystals with maximum dimension larger than 50 µm. The OCS concentrations were compared to 2DC concentrations. The latter were derived by integrating from 50 µm to larger diameters. Cooper and Saunders reported 2DC-OCS concentration ratios between 3.6 and 0.6 ($\overline{x} = 1.7$, $\sigma = 0.9$, number of samples = 12). From the comparisons it was concluded that, for crystals larger than 50 µm, the 2DC is capable of making quantitative concentration measurements.

Based on the findings discussed in the previous paragraph we derived $N_{IC}$ (Table 1) as the diameter-integrated concentration corresponding to $D > 50$ µm. Further, we excluded from our analysis instances when the concentration of crystals in the first 2DC channel (25 to 50 µm) exceeded more than 50 % of the overall ($D > 25$ µm) diameter-integrated concentration. The intent of this criterion is avoidance of crystals whose concentration is uncertain because their depth of field is ambiguous. If we had summed those crystals into $N_{IC}$, the relative concentration bias could have approached a limiting value equal to the ratio of the 2DC manufacturer's recommendation for a 25 to 50 µm particle's depth of field (~ 4 mm) divided by the sampling aperture (61 mm) (Strapp et al., 2001).

For both the PCASP and the 2DC the relative Poisson sampling error was evaluated as the reciprocal of the square root of the particle count.

### 2.3 Air motion

Vertical and horizontal air velocities were derived from differential pressure measurements made at the tip of the King Air's nose boom (Parish and Leon, 2013).

### 2.4 Lidar

The upward-pointing Wyoming Cloud Lidar (Wang et al., 2009, 2012) was used to remotely sense cloud boundaries. The lidar transmits in the near ultraviolet ($\lambda$ = 0.355 µm) at a pulse repetition frequency of 20 Hz. Seven lidar shots were averaged,





ACPD
14, 26591–26618, 2014



making the effective sample rate ~3 Hz. The vertical resolution of the lidar is 3.75 m. Using the lidar measurement of attenuated backscatter and depolarization, we evaluated the boundaries between clear air and liquid cloud, and between liquid-dominated and ice-dominated cloud (Wang and Sassen, 2001).

In the next section we describe our determinations of the air parcel streamlines and how the lidar-derived cloud boundaries were used to evaluate the time interval, along the streamlines, within the liquid-dominated portions of the clouds.

## 3 Analysis

### 3.1 Parcel streamlines and parcel thermodynamic state

Here we explain how the streamlines were derived from measurements made during level-flight penetrations of 35 wave clouds. In our data set we have 19 penetrations made along the wind, and sixteen penetrations made against the wind. Also described is the parcel model we used to evaluate thermodynamic properties along the streamlines.

An average horizontal wind speed ($\overline{u}$) was derived from airborne in-situ wind measurements made during each of the cloud penetrations. That average was applied as a constant in our streamline analysis. In contrast, the in-situ measured vertical wind component ($w$) was oscillatory, so we fitted it as a sinusoid function, vs. along-track distance ($x$), and we assumed that the fitted vertical wind component ($w(x)$) did not vary vertically. Figure 1a shows the measured and fitted values of the vertical wind for a penetration that we showcase to illustrate our methods.

Within the ascending portion of the wave structure (e.g., to the left (upwind) of $x$ = 10.5 km in Fig. 1a), we initialized several streamlines. The streamline center points were separated by ~ 550 m along the flight track (five seconds at 110 m s$^{-1}$). For each of the center points the 1 Hz measurements of $T$, $T_{dp}$, and pressure ($P$) were used to derive five-second averaged values of $T$, $T_{dp}$, and $P$. These three properties were used





ACPD
14, 26591–26618, 2014



to fix an air parcel's initial thermodynamic state. A closed parcel model, conserving potential temperature below the lifted condensation level (LCL), and equivalent potential temperature, above the LCL, was used to evaluate the thermal state, along the streamline. Using this model, and the aforementioned descriptions of the horizontal and vertical wind components, we simulated the thermal and kinematic evolution of streamline-following air parcels. One of the evaluated relationships is the parcel's temperature as a function of the along-track distance. ~~This is shown, for the example, in Fig. 1d.~~ Also indicated are the minimum streamline temperature ($T_{low}$) and the measurement of temperature (red circle) made at the downwind intersection of the flight track and the streamline.

We compared our streamline temperatures, each evaluated at the downwind track-streamline intersections, and the corresponding measured temperatures. The average absolute difference is 0.3 °C (number of samples = 80). This agreement is consistent with a small effect, smaller than the temperature measurement error (±0.5 °C), coming from violations of either the closed parcel assumption or the assumptions of vertically-uniform $w(x)$ and constant $\overline{u}$.

### 3.2 Mixed-phase time

The interval of time an air parcel experiences water-saturated conditions was evaluated by combining the lidar measurements with the streamline information. We refer to this time interval as the mixed-phase time ($t_{MP}$). Figure 1b and c illustrate how $t_{MP}$ was evaluated. At the upwind cloud edge, at $x = 9.5$ km but above the aircraft, the streamline encounters the first of two cloud boundaries. Using lidar measurements, we defined this upwind cloud boundary by its increased lidar backscatter and decreased lidar depolarization (compared to the depolarization in clear air). Approximately four km downwind, the streamline encounters the second boundary. We defined this boundary by its decreased lidar backscatter and increased depolarization. Here the boundary is between liquid- and ice-dominated cloud. Further, we defined $t_{MP}$ as the integral of the parcel transit time between these two boundaries. For a few of the streamlines,





ACPD
14, 26591–26618, 2014



the downwind track-streamline intersection was within the liquid-cloud region. In those cases, the calculation of $t_{MP}$ was stopped at the intersection. The lower and upper bounds of $t_{MP}$ are 38 to 507 s; the average $t_{MP}$ is 221 s.

We obtained good agreement between values of $t_{MP}$, based exclusively on lidar, and those based partially on the in-situ measurements of $T$ and $T_{dp}$. These comparisons were made by differencing the lidar-derived $t_{MP}$ and a mixed-phase time derived using $T$- and $T_{dp}$-dependent determinations of the LCL (Sect. 3.1) combined with lidar-based determinations of the downwind cloud boundary. In this comparison the average absolute difference is 22 s. Each absolute difference was converted to a relative difference by dividing by the lidar-derived values of $t_{MP}$. The relative differences range from 0.0 to 0.9.

### 3.3 Aerosol particles and cloud droplets

In this section we evaluate the connection between upwind aerosol concentrations and in-cloud droplet concentrations. For each of the 35 cloud penetrations we evaluated five-second averages of the PCASP and FSSP concentrations. For the PCASP, the averaging interval was started five seconds upwind of the cloud, and for the FSSP, the averaging interval was started at the cloud edge. Averaging intervals are shown at the bottom of Fig. 2b and at the top of Fig. 2d. Also presented (Fig. 2a–c) are the size-resolved concentrations from the PCASP, FSSP and 2DC. The series shown in Fig. 2 are for the same section of flight illustrated in Fig. 1.

Similar to Eidhammer et al. (2010), we compared the upwind aerosol particle concentration ($D > 0.25$ µm; five-second averaged) to the in-cloud droplet concentration ($D > 1.5$ µm; five-second averaged). From the series presented in Fig. 2d, it can be seen that droplets, measured at ∼x = 11 km (i.e., downwind of the cloud edge), were more abundant than aerosol particles measured at $\sim x = 10.5$ km (i.e., upwind of the edge). Following this same averaging procedure, we evaluated a droplet-to-aerosol ratio for 32 of our 35 penetrations; three of the 35 were discarded because the droplets were smaller than the minimum size detectable by the FSSP ($D = 1.5$ µm). In the 32





ACPD
14, 26591–26618, 2014



comparisons, the droplet-to-aerosol concentration ratios were consistently greater than 0.7. These results are consistent with the findings of Eidhammer et al. (2010). A reasonable inference is that the $D > 0.25\,\mu m$ particles are internally mixed, that the mixture's water-soluble fraction promoted the nucleation of the droplets, and that the mixture's water-insoluble fraction promoted ice nucleation, presumably via the condensation and immersion freezing pathways. ~~The effect of ice nucleation on cloud properties is clearly evident at the downwind track-streamline intersection (at $\sim x = 15\,km$), in Fig. 1c (lidar depolarization), and in Fig. 2d (diameter-integrated crystal concentration).~~

### 3.4 $D > 0.5\,\mu m$ aerosol particle and IC concentrations

In addition to the $D > 0.25\,\mu m$ aerosol concentrations, analyzed in the previous section, we also evaluated $n_{0.5}$ (Sect. 1). ~~These were averaged over the five-second time windows used for thermodynamic-property averaging (Sect. 3.1).~~ For the rest of the paper, $n_{0.5}$ is reported as a particle count per standard cubic centimeter ($sccm^{-1}$). Also for the rest of the paper, values of $N_{IC}$ (Table 1) are derived as five-second averages evaluated at the downwind track-streamline intersections (e.g., at $\sim x = 15\,km$ in Fig. 1c), and these are reported as a crystal count per standard liter ($sL^{-1}$).

### 3.5 Data set

In the previous sections we described how values of $N_{IC}$, $n_{0.5}$, $T_{low}$, and $t_{MP}$ were evaluated for each streamline. The subset $\{N_{IC}, n_{0.5}, T_{low}\}$ is the streamline data we used to develop a fit of $N_{IC}$, according to the mathematical form of Eq. (1). However, before fitting our measurement data, we excluded streamlines affected by four effects: (1) an abundance of crystals in the first 2DC channel, (2) homogeneous freezing, (3) crystal sublimation, and (4) variable aerosol particle and crystal concentrations. Conditions for data *inclusion* are: ~~(1) $N_{IC,D<50}/N_{IC,D>25} < 0.5$ (Sect. 2.2),~~ (2) $T_{low} > -35\,^{\circ}C$ (Heymsfield and Miloshevich, 1993), (3) ice saturated, or larger relative humidity, at the downwind track-streamline intersection, and (4) relative Poisson sampling errors





ACPD
14, 26591–26618, 2014



(Sect. 2.2) less than specified thresholds[1]. Out of the 116 streamlines we analyzed, 80 satisfy our data inclusion criteria. The set $\{N_{IC}, n_{0.5}, T_{low}, t_{MP}\}$ is provided for the 80 streamlines in the Supplement.

## 4 Fitted N equations

In this section we show results from fitting our measurement data with both temperature-dependent, and temperature-aerosol-dependent, equations. We start with a solely temperature-dependent fitting equation because many previous cloud modeling studies were based on such a relationship (e.g., Meyers et al., 1992), and because the rate of change of crystal concentration with temperature can have a profound impact on modeled cloud properties (Eidhammer et al., 2009).

We develop the fitting equations using logarithm-transformed crystal and logarithm-transformed aerosol concentrations. The reason for log-transforming the measurements is that we expect errors, in both crystal and aerosol concentration, to be multiplicative in the sense that larger values correspond with larger error and vice versa. Multiplicative error, scaling in proportion to the square root of concentration as predicted by the Poisson probability law (Young, 1962; Rogers and Yau, 1989), was documented by Cai et al. (2013) in their investigations of the PCASP's response to steadily-generated monodisperse test particles.

Figure 3a shows the temperature-dependent fit (i.e., $N_{IC}(T_{low})$) plotted vs. $N_{IC}$. ~~The square of the Pearson correlation coefficient ($r^2$), for this scatter plot, is relatively small and demonstrates that temperature alone, via the fit equation, can only explain 44 % of the $N_{IC}$ variability.~~

[1]The relative Poisson error thresholds adopted for IC concentration and for $n_{0.5}$, were 0.4 and 0.7, respectively. These values cut the distributions of the relative Poisson errors at their 99th percentiles.





ACPD
14, 26591–26618, 2014



In Fig. 3b we plot our 80 fitted values of $N_{IC}(T_{low}, n_{0.5})$ vs. $N_{IC}$. Results shown here are for one of two fitting methods we implemented. In fit method #1 we used the Matlab Curve Fitting Toolbox (The MathWorks, Natick, MA), with the log-transformed version of Eq. (1), and derived the logarithm of $a$ ($\ln a$), and the values of $b$, $c$ and $d$. We also fitted our 80 measurements of $\{N_{IC}, n_{0.5}, T_{low}\}$ using the ~~procedure described in D10.~~ We refer to the latter as method #2. The advantage of method #1 is that it shortens D10's three-step procedure to one step. ~~Another difference is that the number of points used to evaluate statistical error, associated with the fit coefficients, is relatively small in the case method #2. In method #1 the number of points is 80, while in our application of method #2 only four points were fitted in the second and third steps of D10's procedure.~~

The fit coefficients derived by D10, our fit coefficients (methods #1 and #2), and the method #1 and #2 statistical errors, expressed as standard deviations, are presented in Table 2. ~~Focusing on results obtained using method #1, our coefficients $\ln a$ and $b$, and our coefficients $c$ and $d$, are seen to agree within one and two standard deviations of D10's, respectively. Also, there is agreement, within one standard deviation, between our application of method #2 and D10's. It is also apparent that larger statistical error is evident for $\ln a$ and $b$ derived in method #2, compared to method #1. This is because of the smaller number of points fitted in method #2, as discussed in the previous paragraph.~~

By inputting the statistical errors from Table 2 into a propagation of error equation (Young, 1962; their Eq. 13.9), we evaluated contributions to the relative variance of the logarithm of $N_{IC}(T_{low}, n_{0.5})$ (method #1). For $n_{0.5} \leq 3.4\,\mathrm{sccm}^{-1}$ (the average for our data set), and for temperatures over the full range of our data set ($-34 \leq T_{low} \leq -14\,^{\circ}\mathrm{C}$), the relative variance is controlled by terms proportional to both the square of the statistical error in $\ln a$ and the square of the statistical error in $b$. Further, we also evaluated the fractional standard deviation of $N_{IC}(T_{low}, n_{0.5})$ (method #1). For the same $n_{0.5}$ and $T_{low}$ settings provided above, the fractional standard deviation is $\sim 4$ and increases to $\sim 5$ if $n_{0.5}$ is set to $16\,\mathrm{sccm}^{-1}$ (the maximum for our data set). Yet, in spite of this uncertainty, our fitted (method #1) and measured values are seen to correlate over three decades





ACPD
14, 26591–26618, 2014



of IC concentration (Fig. 3b). Also illustrated are fitted concentrations, derived using Eq. (1) with D10's coefficients and our measurements of $T_{low}$ and $n_{0.5}$ In either case the $r^2$ is ~ 0.7 and thus larger than that for the temperature-only fit (cf., Fig. 3a).

We also evaluated the fraction of the measured crystal concentrations that plot within a factor of two of the fit. ~~Based on our method #1 coefficients, this percentage is 69 % and thus larger than the percentage (66 %) based on fit coefficients from D10 (the percentage is 60 % when using the method #2 coefficients; not shown here). Thus, we obtained better fitted-vs.-measured agreement with our method #1 fit coefficients, and poorer agreement with either our method #2 coefficients or with the D10 coefficients.~~

## 5 Effect of mixed-phase time

~~As was discussed in the introduction, there is an outstanding question in atmospheric science community regarding the time-dependent nature of ice nucleation. Of relevance for our data set, with its average $t_{MP}$ = 221 s (Sect. 3.2), is the possibility that the characteristic time for a subcritical ice embryo to transition to a detectable ice particle is comparable to $t_{MP}$. If that were the case, we would expect that streamlines associated with larger mixed-phase times, all other things equal, would have larger IC concentrations. We explored this by stratifying our 80 determinations of $\{N_{IC}, n_{0.5}, T_{low}, t_{MP}\}$ into four $T_{low}$ subsets.~~ In Table 3 we present the subset's minimum and maximum temperatures, the averaged $n_{0.5}$, and the number of data values. For each of these we tested the hypothesis that $\ln(N_{IC})$ is correlated with $\ln(t_{MP})$. Values of the Pearson correlation coefficients ($r$), and the levels of significance ($p$), demonstrate that none of the correlations are significant (i.e., all have $p > 0.05$). This same conclusion was reached after removing from the correlations those points exhibiting the largest $t_{MP}$ uncertainty (relative difference > 0.3, Sect. 3.2), but those results are not shown in Table 3. We also stratified by $n_{0.5}$ within the four $T_{low}$ subsets. One of those correlations ($\ln(N_{IC})$ vs. $\ln(t_{MP})$) approaches statistical significance, with $p = 0.1$ and with 10 paired values; the





ACPD
14, 26591–26618, 2014



rest have $p > 0.1$. That subset plots in the gray rectangle shown in Fig. 4a and the $N_{IC}$ vs. $t_{MP}$ correlation for that subset is shown in Fig. 4b.

~~In spite of these suggestions of a connection between crystal concentration and mixed-phase time we cannot argue convincingly that time-dependent effects were significant for crystals within the clouds we studied. Our ability to argue for, or against a dependence on $t_{MP}$, was limited by the number of points within the analyzed data subsets. Thus, in future wave cloud studies, attention should be paid to strategies which generate an adequate number of points within specified temperature and aerosol ranges.~~

## 6 Summary and conclusion

~~The result we present in Table 2, with fit coefficients generally consistent, in a statistical sense, with those reported by D10, is significant because it validates D10's equation using different methodology.~~ In short, our technique uses a streamline model to connect a measurement of aerosol concentration ($n_{0.5}$), made upwind of a wave cloud, to a downwind measurement of IC concentration. Our reconfirmation of the connection between crystals and $n_{0.5}$ – the connection implied by Eq. (1) – is conceptually appealing because it acknowledges that aerosol particles are necessary for the occurrence of heterogeneous ice nucleation. Appeal also comes from the linkage provided by Eq. (1), through aerosol, to cloud processes.

~~We also probed the conjecture that the duration of nuclei exposure to water-saturated conditions is a determinant of IC concentration.~~ Our analysis shows no statistically-robust evidence for this. This finding is relevant to descriptions of ice nucleation within water-saturated layer clouds (e.g., stratocumulus and altostratus) where temperature is relatively uniform, and steady, and where time-dependent ice nucleation is suspected of occurring continuously and with substantial meteorological impact (Crosier et al., 2011; Westbrook and Illingworth, 2013). In fact, many model representations of heterogeneous nucleation anticipate this time-dependent, constant-temperature, phenomenon.





ACPD
14, 26591–26618, 2014



Also, in some models, the nucleation rate is set to zero when the temperature tendency is zero or positive (Khain et al., 2000; Muhlbauer and Lohmann, 2009), but this action is not supported by all of the experimental evidence currently available (for a review, see Vali, 2014). Further investigation is needed to confirm our conclusion of little, if any, time-dependent effect within the cloud type we studied (middle-tropospheric wave clouds). Going forward, we anticipate our methodology will help advance understanding of time-dependent atmospheric ice nucleation, and atmospheric ice nucleation in general.

**The Supplement related to this article is available online at doi:10.5194/acpd-14-26591-2014-supplement.**

*Acknowledgements.* The data collection and initial analyses were supported by NSF under Award AGS-0645644. The authors thank Alfred Rodi, Jeffrey French, Larry Oolman, Matthew Burkhart and Perry Wechsler for the assistance they provided during the field and analysis phases of the project. The authors also thank Paul DeMott who critiqued an early draft of the paper. JRS acknowledges support from NSF grant AGS1034858.

## References

Baumgardner, D., Strapp, W., and Dye, J. E.: Evaluation of the forward scattering spectrometer probe. Part II: Corrections for coincidence and dead-time losses, J. Atmos. Ocean. Tech., 2, 626–632, 1985.

Bigg, E. K.: The supercooling of water, P. Phys. Soc. Lond. B, 66, 688–694, 1953.

Braham, R. R. and Squires, P.: Cloud Physics-1974, B. Am. Meteorol. Soc., 55, 543–586, 1974.

Cai, Y., Snider, J. R., and Wechsler, P.: Calibration of the passive cavity aerosol spectrometer probe for airborne determination of the size distribution, Atmos. Meas. Tech., 6, 2349–2358, doi:10.5194/amt-6-2349-2013, 2013.

Cantrell, W. and Heymsfield, A.: Production of ice in tropospheric clouds: a review, B. Am. Meteorol. Soc., 86, 795–807, 2005.





ACPD
14, 26591–26618, 2014



Cooper, W. A. and Saunders, C. P. R.: Winter storms over the San Juan Mountains. Part II: Microphysical processes, J. Appl. Meteorol., 19, 927–941, 1980.
Cooper, W. A. and Vali, G.: The origin of ice in mountain cap clouds, J. Atmos. Sci., 38, 1244–1259, 1981.
Crosier, J., Bower, K. N., Choularton, T. W., Westbrook, C. D., Connolly, P. J., Cui, Z. Q., Crawford, I. P., Capes, G. L., Coe, H., Dorsey, J. R., Williams, P. I., Illingworth, A. J., Gallagher, M. W., and Blyth, A. M.: Observations of ice multiplication in a weakly convective cell embedded in supercooled mid-level stratus, Atmos. Chem. Phys., 11, 257–273, doi:10.5194/acp-11-257-2011, 2011.
Cotton, R. and Field, P.: Ice nucleation characteristics of an isolated wave cloud, Q. J. Roy. Meteor. Soc., 128, 2417–2437, 2002.
DeMott, P. J., Prenni, A. J., Liu, X., Kreidenweis, S. M., Petters, M. D., Twohy, C. H., Richardson, M. S., Eidhammer, T., and Rogers, D. C.: Predicting global atmospheric ice nuclei distributions and their impacts on climate, P. Natl. Acad. Sci. USA, 107, 11217–11222, 2010.
DeMott, P. J., Prenni, A. J., McMeeking, G. R., Sullivan, R. C., Petters, M. D., Tobo, Y., Niemand, M., Möhler, O., Snider, J. R., Wang, Z., and Kreidenweis, S. M.: Integrating laboratory and field data to quantify the immersion freezing ice nucleation activity of mineral dust particles, Atmos. Chem. Phys. Discuss., 14, 17359–17400, doi:10.5194/acpd-14-17359-2014, 2014.
Dobosy, R. J., Crawford, T. L., MacPherson, J. I., Desjardins, R. L., Kelly, R. D., Oncley, S. P., and Lenschow, D. H.: Intercomparison among four flux aircraft at BOREAS in 1994, J. Geophys. Res., 102, 29101–29111, 1997.
Eidhammer, T., DeMott, P. J., and Kreidenweis, S. M.: A comparison of heterogeneous ice nucleation parameterizations using a parcel model framework, J. Geophys. Res., 114, D06202, doi:10.1029/2008JD011095, 2009.
Eidhammer, T., DeMott, P. J., Prenni, A. J., Petters, M. D., Twohy, C. H., Rogers, D. C., Stith, J., Heymsfield, A., Wang, Z., Pratt, K. A., Prather, K. A., Murphy, S. M., Seinfeld, J. H., Subramanian, R., and Kreidenweis, S. M.: Ice initiation by aerosol particles: measured and predicted ice nuclei concentrations versus measured ice crystal concentrations in an orographic wave cloud, J. Atmos. Sci., 67, 2417–2436, 2010.
Field, P. R., Wood, R., Brown, P. R. A., Kaye, P. H., Hirst, E., Greenaway, R., and Smith, J. A.: Ice particle interarrival times measured with a fast FSSP, J. Atmos. Ocean. Tech., 20, 249–261, 2003.





ACPD
14, 26591–26618, 2014



Field, P. R., Heymsfield, A. J., Shipway, B. J., DeMott, P. J., Pratt, K. A., Rogers, D. C., Stith, J., and Prather, K. A.: Ice in clouds experiment-layer clouds. Part II: Testing characteristics of heterogeneous ice formation in lee wave clouds, J. Atmos. Sci., 69, 1066–1079, 2012.
Gardiner, B. A. and Hallett, J.: Degradation of in-cloud forward scattering spectrometer probe measurements in the presence of ice particles, J. Atmos. Ocean. Tech., 2, 171–180, 1985.
Gayet, J. F., Febvre, G., and Larsen, H.: The reliability of the PMS FSSP in the presence of small tee crystals, J. Atmos. Ocean. Tech., 13, 1300–1310, 1996.
Hoose, C., Kristjánsson, J. E., Chen, J.-P., and Hazra, A.: A classical-theory-based parameterization of heterogeneous ice nucleation by mineral dust, soot and biological particles in a global climate model, J. Atmos. Sci., 67, 2483–2503, 2010.
Heymsfield, A. J., Miloshevich, L. M.: Homogeneous ice nucleation and supercooled liquid water in orographic wave clouds, J. Atmos. Sci., 50, 2335–2353, 1993.
Khain, A. P., Ovtchinnikov, M., Pinsky, M., Pokrovsky, A., and Krugliak, H.: Notes on the state-of-the-art numerical modeling of cloud microphysics, Atmos. Res., 55, 159–224, 2000.
Korolev, A. V. and Isaac, G. A.: Shattering during sampling by OAPs and HVPS. Part I: Snow particles, J. Atmos. Ocean. Tech., 22, 528–542, 2005.
Korolev, A. V., Emery, E. F., Strapp, J. W., Cober, S. G., and Isaac, G. A.: Quantification of the effects of shattering on airborne ice particle measurements, J. Atmos. Ocean. Tech., 30, 2527–2553, 2013.
Lawson, R. P. and Cooper, W. A.: Performance of some airborne thermometers in clouds, J. Atmos. Ocean. Tech., 7, 480–494, 1990.
Meyers, M. P., DeMott, P. J., and Cotton, W. R.: New primary ice-nucleation parameterizations in an explicit cloud model, J. Appl. Meteorol., 31, 708–721, 1992.
Muhlbauer, A. and Lohmann, U.: Sensitivity studies of aerosol–cloud interactions in mixed-phase orographic precipitation, J. Atmos. Sci., 66, 2517–2538, 2009.
Murray, B. J., O'Sullivan, D., Atkinson, J. D., and Webb, M. E.: Ice nucleation by particles immersed in supercooled cloud droplets, Chem. Soc. Rev., 41, 6519–6554, 2012.
Niemand, M., Möhler, O., Vogel, B., Vogel, H., Hoose, C., Connolly, P., Klein, H., Bingemer, H., DeMott, P., Skrotzki, J., and Leisner, T.: A particle-surface-area-based parameterization of immersion freezing on desert dust particles, J. Atmos. Sci., 69, 3077–3092, 2012.
Parish, T. R. and Leon, D.: Measurement of cloud perturbation pressures using an instrumented aircraft, J. Atmos. Ocean. Tech., 30, 215–229, 2013.





ACPD
14, 26591–26618, 2014



Pokharel, B. and Vali, G.: Evaluation of collocated measurements of radar reflectivity and particle sizes in ice clouds, J. Appl. Meteorol., 50, 2104–2119, 2011.
Rodi, A. R. and Spyers-Duran, P. A.: Analysis of time response of airborne temperature sensors, J. Appl. Meteorol., 11, 554–556, 1972.
Rogers, R. R. and Yau, M. K.: A Short Course in Cloud Physics, 3rd ed. Permagon Press, 304 pp., 1989.
Rogers, D. C., DeMott, P. J., Kreidenweis, S. M., and Chen, Y. L.: A continuous-flow diffusion chamber for airborne measurements of ice nuclei, J. Atmos. Ocean. Tech., 18, 725–741, 2001.
Snider, J. R. and Petters, M. D.: Optical particle counter measurement of marine aerosol hygroscopic growth, Atmos. Chem. Phys., 8, 1949–1962, doi:10.5194/acp-8-1949-2008, 2008.
Snider, J. R., Leon, D., and Wang, Z.: Southeast pacific stratocumulus cloud droplet concentrations. Part I – Modeled, retrieved, and directly-observed values, J. Atmos. Sci., in review, 2014.
Strapp, J. W., Leaitch, W. R., and Liu, P. S. K.: Hydrated and dried aerosol-size-distribution measurements from the particle measuring systems FSSP-300 probe and the deiced PCASP-100× Probe, J. Atmos. Ocean. Tech., 9, 548–555, 1992.
Strapp, J. W., Albers, F., Reuter, A., Korolev, A. V., Maixner, U., Rashke, E., and Vukovic, Z.: Laboratory measurements of the response of a PMS OAP-2DC, J. Atmos. Ocean. Tech., 18, 1150–1170, 2001.
Wang, Z. and Sassen, K.: Cloud type and macrophysical property retrieval using multiple remote sensors, J. Appl. Meteorol., 40, 1665–1682, 2001.
Wang, Z., Wechsler, P., Kuestner, W., French, J., Rodi, A., Glover, B., Burkhart, M., and Lukens, D.: Wyoming Cloud Lidar: instrument description and applications, Opt. Express, 17, 13576–13587, 2009.
Wang, Z., French, J., Vali, G., Wechsler, P., Haimov, S., Rodi, A., Deng, M., Leon, D., Snider, J., and Peng, L.: Single aircraft integration of remote sensing and in situ sampling for the study of cloud microphysics and dynamics, B. Am. Meteorol. Soc., 93, 653–668, 2012.
Westbrook, C. D. and Illingworth, A. J.: The formation of ice in a long-lived supercooled layer cloud, Q. J. Roy. Meteor. Soc., 139, 2209–2221, 2013.
Wright, T. P., Petters, M. D., Hader, J. D., Morton, T., and Holder, A. L.: Minimal cooling rate dependence of ice nuclei activity in the immersion mode, J. Geophys. Res., 118, 10535–10543, doi:10.1002/jgrd.50810, 2013.





ACPD
14, 26591–26618, 2014



Vali, G.: Nucleation terminology, B. Am. Meteorol. Soc., 66, 1426–1427, 1985.
Vali, G.: Interpretation of freezing nucleation experiments: singular and stochastic; sites and surfaces, Atmos. Chem. Phys., 14, 5271–5294, doi:10.5194/acp-14-5271-2014, 2014.
Vali, G. and Stansbury, E. J.: Time-dependent characteristics of the heterogeneous nucleation of ice, Can. J. Phys., 44, 477–502, 1966.
Vali, G., Politovich, M. K., and Baumgardner, D. G.: Conduct of cloud spectra measurements, Report AFGL-TR-81-0122, Air Force Geoph. Lab., Available from Nat'l. Techn. Inf. Serv., Order No. AD-A102944/6, 1981.
Young, H. D.: Statistical Treatment of Experimental Data, McGraw-Hill Book Company, 107 pp., 1962.





ACPD
14, 26591–26618, 2014



**Table 1.** Symbols used to represent aerosol, IN and IC concentrations.

| Symbol | Definition | Dimension |
|---|---|---|
| $n_{0.5}$ | Measured aerosol concentration ($D > 0.5\,\mu m$) | $sccm^{-1}$ [a] |
| $N_{IC}$ | Measured IC concentration ($D > 50\,\mu m$) [b] | $sL^{-1}$ [c] |
| $N_{IC}(T)$ | Temperature-dependent fit of IC concentration (see Sect. 4) | $sL^{-1}$ |
| $N_{IC}(T, n_{0.5})$ | Temperature- and aerosol-dependent fit of IC concentration (see Sect. 4) | $sL^{-1}$ |
| $N_{IN}(T, n_{0.5})$ | Temperature- and aerosol-dependent fit of IN concentration (D10) (see Eq. 1) | $sL^{-1}$ |

[a] Aerosol particle count per standard cubic centimeter at $P = 1.013 \times 10^5$ Pa and $T = 273.15$ K;
[b] 2DC concentration for crystals sizing larger than 50 µm (see Sect. 2.2);
[c] Particle count per standard liter at $P = 1.013 \times 10^5$ Pa and $T = 273.15$ K.





ACPD
14, 26591–26618, 2014



**Table 2.** Equation (1) fit coefficients.

| Coefficients | Fit D10[a] | Fit Method #1 | Statistical Error[b] Method #1 | Fit Method #2 | Statistical Error[c] Method #2 |
|---|---|---|---|---|---|
| ln *a* | −9.73 | ~~−14.89~~ | ~~2.93~~ | ~~−8.67~~ | ~~6.65~~ |
| *b* | 3.33 | ~~4.79~~ | ~~0.89~~ | ~~2.86~~ | ~~2.21~~ |
| *c* | 0.0264 | ~~0.0076~~ | ~~0.0313~~ | ~~0.0225~~ | ~~0.027~~ |
| *d* | 0.0033 | 0.86 | ~~0.89~~ | ~~0.49~~ | ~~0.68~~ |

[a] Fit coefficients from D10;
[b] The standard deviations for coefficients fitted via method #1;
[c] The standard deviations for coefficients fitted via method #2.





ACPD
14, 26591–26618, 2014



**Table 3.** $T_{low}$ subsets and the $\ln(N_{IC})$ vs. $\ln(t_{MP})$ correlations.

| $T_{min}$ | $T_{max}$ | $\overline{n_{0.5}}$ | Number of samples | $r$[a] | $p$[b] |
|---|---|---|---|---|---|
| −34 | −29 | 5.50 | 20 | 0.20 | 0.20 |
| −29 | −24 | 2.88 | 30 | 0.21 | 0.13 |
| −24 | −19 | 3.50 | 15 | −0.05 | 0.57 |
| −19 | −14 | 2.57 | 15 | 0.06 | 0.44 |

[a] The Pearson correlation coefficient for the regression of $\ln(N_{IC})$ vs. $\ln(t_{MP})$;
[b] Level of significance, values of this parameter greater than $p = 0.05$ indicate an insignificant correlation.





ACPD
14, 26591–26618, 2014



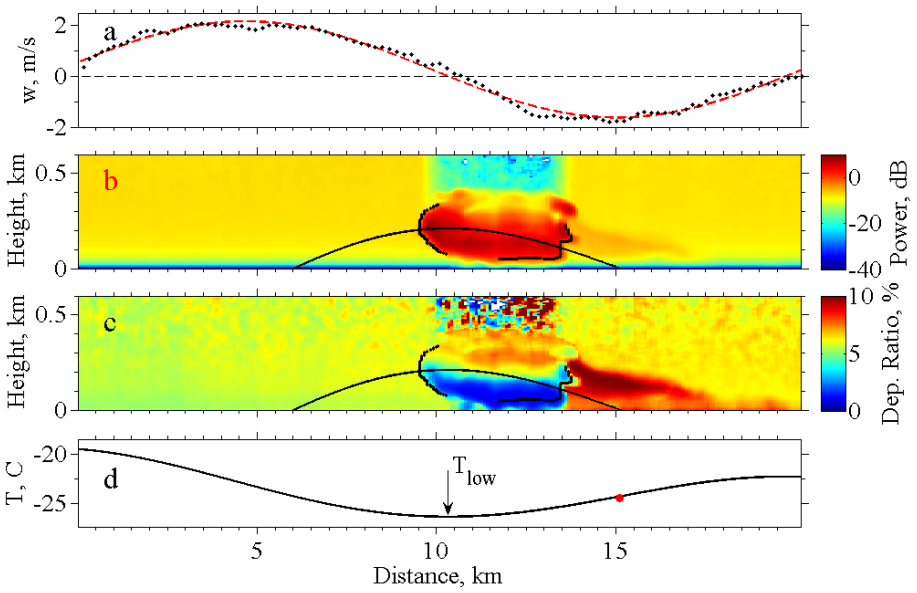


**Figure 1.** Airborne level-flight sampling a few tens of meter below a wave cloud between 18:17:45 and 18:20:09 on 27 February 2008. Airflow is from left to right. **(a)** In-situ vertical velocity measurements and the sinusoid fit. **(b)** The example streamline (black) overlain on lidar backscattered power; the two other black lines delineate the liquid-cloud and ice-cloud boundaries discussed in the text. **(c)** Example streamline overlain on lidar depolarization ratio; the two other black lines delineate the liquid-cloud and ice-cloud boundaries discussed in the text. **(d)** Streamline temperature, minimum streamline temperature, and the in-situ measured temperature at the downwind track-streamline intersection (red circle).





ACPD
14, 26591–26618, 2014



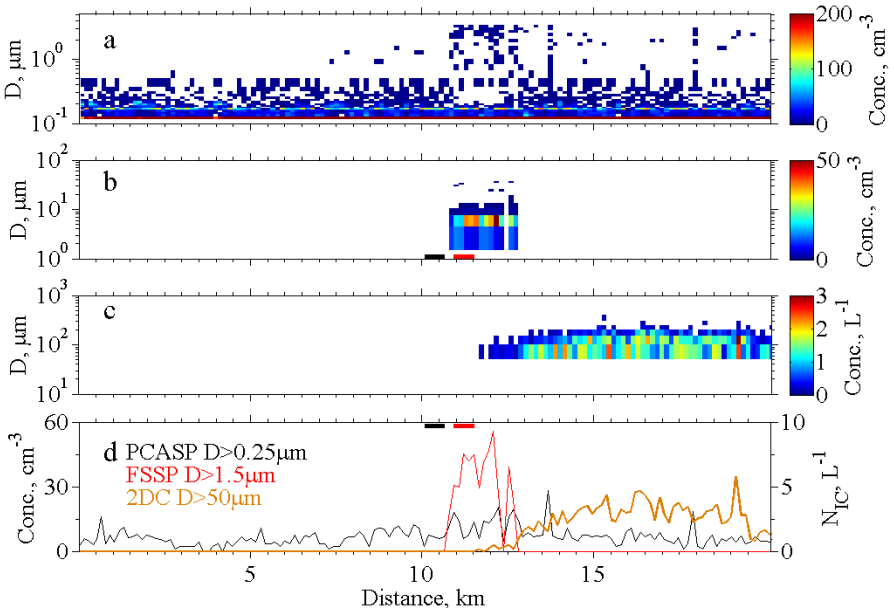


**Figure 2.** The same segment of flight as shown in Fig. 1; **(a)** Size-resolved PCASP concentrations. **(b)** Size-resolved FSSP concentrations. The black and red horizontal rectangles at the bottom of this panel are the five-second averaging intervals for aerosol and droplets analyzed in Sect. 3.3. **(c)** Size-resolved 2DC concentrations. **(d)** Diameter-integrated PCASP ($D > 0.25\,\mu m$, black line), diameter-integrated FSSP ($D > 1.5\,\mu m$, red line), and diameter-integrated 2DC ($D > 50\,\mu m$, orange line) concentrations. Averaging intervals for aerosol and droplets are repeated from panel b.





ACPD
14, 26591–26618, 2014



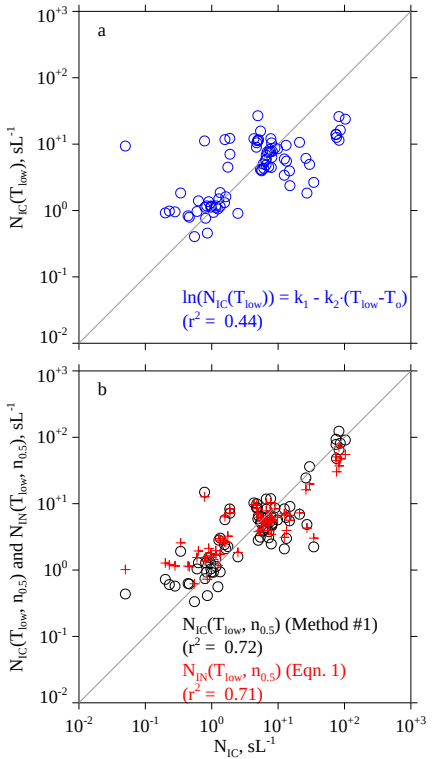


**Figure 3. (a)** ~~Values of $N_{IC}(T_{low})$ ($\ln(N_{IC}(T_{low})) = k_1 - k_2 \cdot (T_{low} - T_o)$ with $k_1 = -3.93$ and $k_2 = 0.22\ °C^{-1}$~~) plotted vs. $N_{IC}$. **(b)** As in Fig. 3a, but with $N_{IC}(T_{low}, n_{0.5})$ (method #1 fit coefficients), and $N_{IN}(T_{low}, n_{0.5})$ (Eq. 1), plotted vs. $N_{IC}$. In Fig. 3a and b, the square of the Pearson correlation coefficients ($r^2$) was evaluated using log-transformed concentrations. Also, the one-to-one line is shown in both panels.





ACPD
14, 26591–26618, 2014



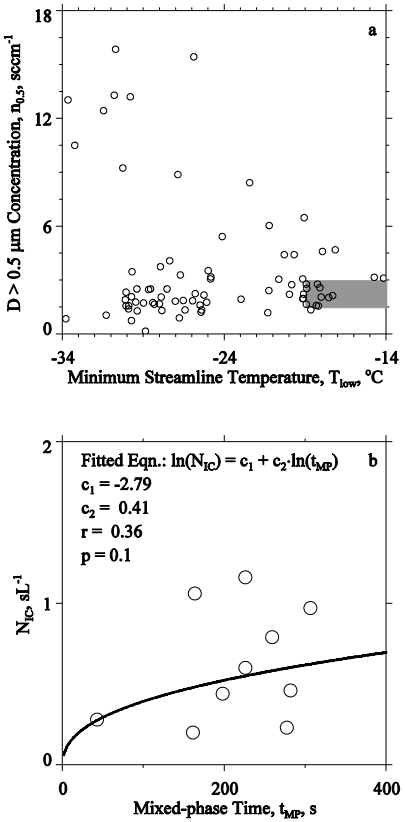


**Figure 4. (a)** The 80 paired values of $n_{0.5}$ and $t_{MP}$ in our data set. The gray rectangle highlights the 10 points in the subset defined by $-19 \le T_{low} < -14$ °C and $1.5 \le n_{0.5} < 3.0\,\mathrm{sccm}^{-1}$. **(b)** The 10 paired values of $N_{IC}$ and $t_{MP}$ from the gray rectangle shown in Fig. 4a. The black line is the fitting equation $\ln(N_{IC}) = c_1 + c_2 \cdot \ln(t_{MP})$. The Pearson correlation coefficients ($r$), and the level of significance ($p$), were evaluated using the log-transformed concentrations and log-transformed mixed-phase times.





ACPD
14, 26591–26618, 2014



**Appendix A**

In this appendix we examine the reliability of ice crystal concentrations derived using the University of Wyoming 2DC. We derive concentrations using the Wyoming 2DC, with its slower-responding photodiode array (Gayet et al., 1993; Baumgardner and Korolev, 1997; Strapp et al., 2001), and compare to values derived using a faster responding cloud imaging probe (CIP; Baumgardner et al., 2001). We also analyze the 2DC ice crystal interarrival times and investigate crystal shattering. Two data sets are analyzed. The first comes from Wyoming King Air flight data, acquired on 9 January 2011 during the Colorado Airborne Multi-Phase Cloud Study (CAMPS), and the second comes from the 80 downwind track-streamline intersections described in Sect. 3.5. Both the 2DC and CIP were operated with standard probe tips (Korolev et al., 2013).

Strapp et al. (2001) conducted laboratory studies that investigated a 2DC's ability to detect objects (circular dots) positioned away from the center of focus of the probe's laser. They demonstrated that the probe's finite response led to undersizing, counting losses and image distortion. At dot sizes smaller than 100 μm, undersizing and counting losses increased with the speed the dots transited through the probe's sample volume. Strapp et al. conducted their testing using dots deposited onto a glass disk. The dots were opaque, monodisperse, and regularly spaced on the disk along circular tracks. The disk was positioned with its rotational axis parallel to the 2DC laser beam. The position of the disk plane, relative to the center of focus of the beam, was varied. The largest dot speeds tested by Strapp et al. were comparable to the airspeed of the Wyoming King Air (~100 m/s).

**A1 - 2DC and CIP Concentrations**

A comparison of 2DC- and CIP-derived concentrations was made using Wyoming King Air data acquired on 9 January, 2011 (20110109). The comparison data was selected from three level-flight transits of an orographic cloud. The cloud was located over continental divide in northern Colorado. During the cloud transits the liquid water content was less than 0.2 g $m^{-3}$ and temperature was between -23 and -25 $^{o}$C. We processed the raw 2DC and CIP measurements the same way we processed the WAICO 2DC measurements (Sect. 2.2). Also consistent with the WAICO

28 processing, the compared concentrations are five-second averages and are for crystals larger than
29 50 μm (sized along the aircraft track). The CIP/2DC comparison is shown in Fig. A1a. The vertical line
30 at 5 $L^{-1}$ marks the median of the 80 concentrations in our WAICO data set (Sect. 3.5), and its
31 implication is discussed in the following paragraph.

32 Because of the undersizing and counting losses documented for a 2DC, especially at the low
33 end of its range (D < 100 μm), and the fact these effects are attributed to the relatively slow time
34 response of the 2DC's optical array (Strapp et al., 2001), it is expected that concentrations derived
35 using the faster responding CIP (Baumgardner et al., 2001) should exceed 2DC-derived values.
36 Contrary to that expectation, we found reasonable agreement (Fig. A1a). Measures of the
37 agreement are as follows: 1) For concentrations larger than 5 $sL^{-1}$, all of the 2DC-derived values plot
38 well within a factor of two of the CIP. 2) For concentrations smaller than 5 $sL^{-1}$, a large fraction of
39 the 2DC values (87%) plot within a factor of two of the CIP. These findings, combined with the
40 findings of Cooper and Saunders (1980) (also see Sect. 2.2), lend confidence to the concentration
41 values we derived using 2DC measurements made during WAICO. However, this comparison does
42 not completely lessen the concern that we biased the WAICO concentrations at D < 100 μm by
43 assuming that the 2DC's optical depth of field was independent of crystal size and equal to the
44 probes's sampling aperture (61 mm) (Vali et al., 1981 and Sect. 2.2).

45 **A2 - Interarrival Time and Shattering**

46 Representative CIP and 2DC size distributions, from CAMPS, are shown in Fig. A1b. It is
47 evident that most of the detected crystals are smaller than 400 μm, especially in the 2DC
48 measurement. A size distribution from one of the 80 WAICO downwind track-streamline
49 intersections is shown in Fig. A2a. The largest crystal detected in this five-second interval is 400
50 μm. A histogram of crystal interarrival times for the same five-second interval is shown in Fig. A2b.
51 Evident in the left tail of the histogram is a minimum, at interarrival time $\tau^*$ = 2x$10^{-3}$ s, where we
52 delineate between a fragment mode ($t < \tau^*$) and a mode corresponding to intact crystals ($t > \tau^*$).
53 We note that 7% of the crystal counts classify as fragments and that this fraction is much smaller

54 than the example presented by Korolev et al. (2013) for a 2DC with standard probe tips (their Fig.
55 14a).

56 We analyzed interarrival times obtained from each of the 80 WAICO downwind track-
57 streamline intersections. Histograms were binned as in A2b (3.5 bins per decade) and all particle
58 images, including those that did not pass the rejection criteria of Pokharel and Vali (2011) (Sect.
59 2.2), were used. We developed a procedure that searches the histogram for a minimum between $t$
60 = $10^{-6}$ s and the histogram mode. In our set of 80 there are 16 cases that do not exhibit a minimum
61 and 21 with a provisionally significant minimum. The provisional cases were characterized by a
62 cumulative fraction, evaluated at the minimum, greater than 20%. The example shown in Fig. A2b
63 is not a provisional case because the cumulative fraction at $\tau^*$ = 2x$10^{-3}$ s is less than 20%. All of the
64 provisional cases exhibited a minimum that was within an order of magnitude of the histogram
65 mode. Because order-of-magnitude separation is substantially less than the minimum-to-mode
66 separation seen Korolev et al. (2013) (their Fig. 14), we concluded that a fragment mode could not
67 be discerned. Thus, we ignored the effect of shattering. Twenty six of the remaining 43 cases
68 (43=80-16-21) had a minimum more than an order of magnitude smaller than the histogram mode;
69 Fig. A2b is an example. For these we ignored the effect of shattering because the fraction affected
70 was less than 20% and because the rejection criteria of Pokharel and Vali (2011) removes some of
71 the affected crystals from the population used to evaluate the concentration.

72

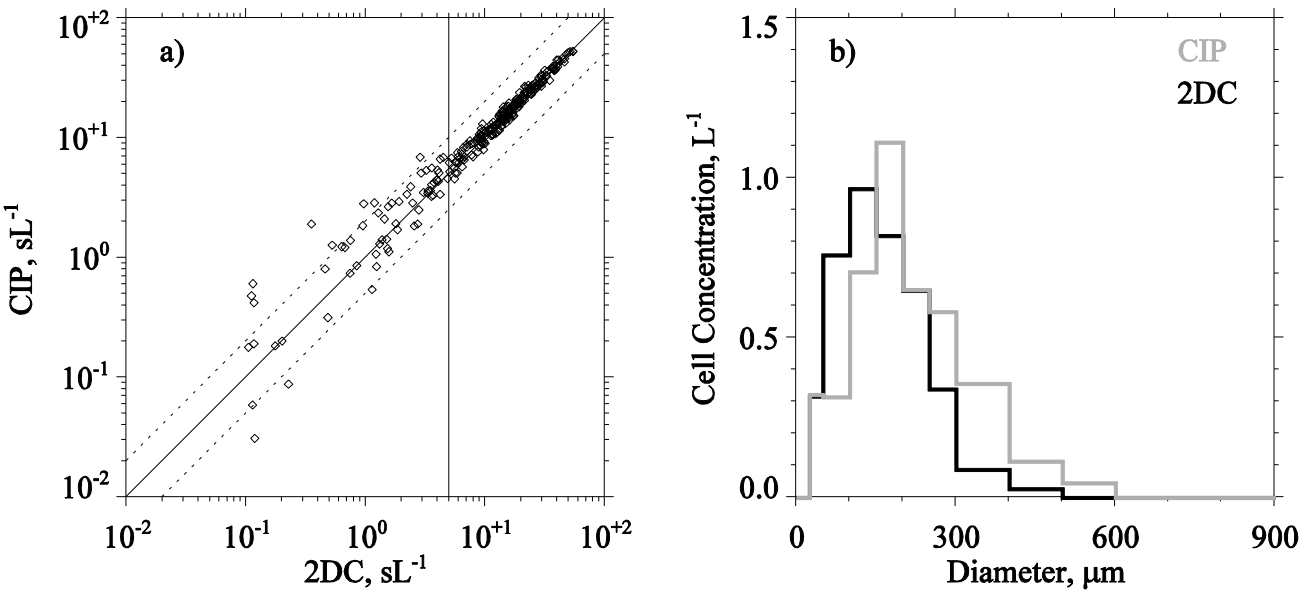


Fig. A1 – a) The CIP/2DC concentration comparison. Compared values are five-second averages and are for crystals larger than 50 µm. Comparison data is from 20110109 during the Colorado Airborne Multi-Phase Cloud Study (CAMPS). Wyoming King Air data shown here was selected from three along-wind level-flight cloud transits: 1) 221200 to 222200 UTC, 2) 223900 to 224800 UTC, and 3) 230600 to 231600 UTC. The vertical line at 5 $sL^{-1}$ is drawn at the median value for our set of 80 WAICO 2DC-derived measurements. b) 2DC and CIP size distributions from a representative five-second subset (224646 to 224650 UTC) of the CAMPS cloud transits on 20110109.

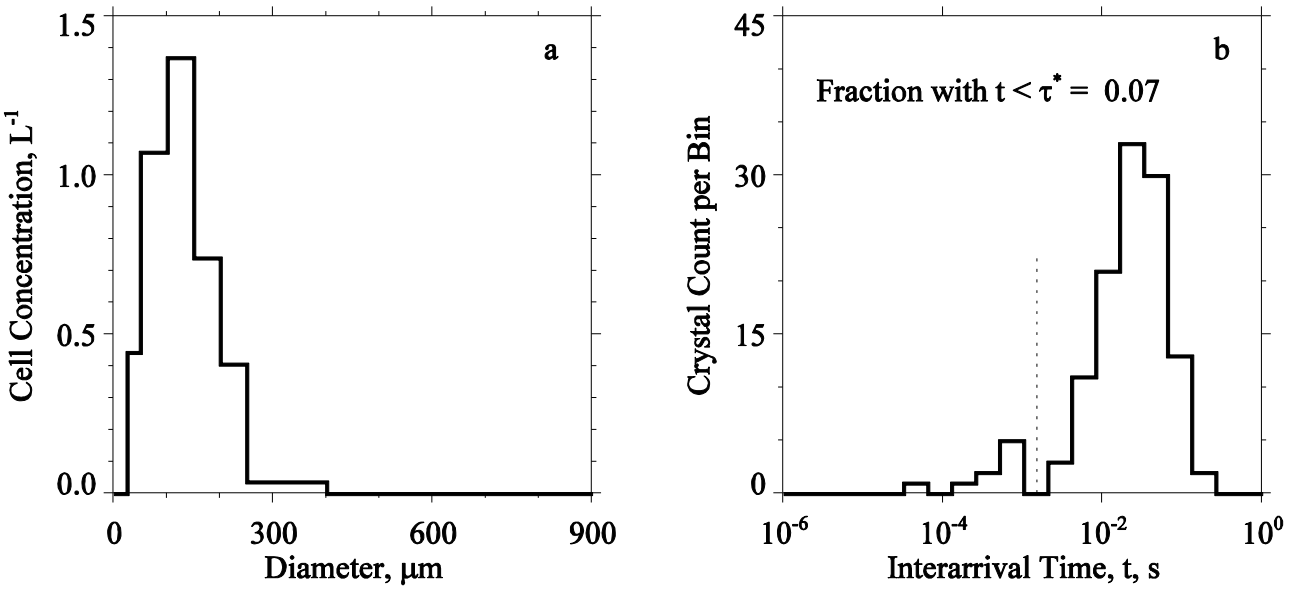


Fig. A2 – a) The 2DC size distribution derived for the WAICO 181933 to 181937 interval on 20080227. This interval corresponds to the downwind track-streamline intersection at x=15 km in Fig. 1c. b) The interarrival time histogram for the 181933 to 181937 interval on 20080227. The vertical dashed line marks a minimum between a fragment mode ($t < \tau^*$) and a mode corresponding to intact crystals ($t > \tau^*$).

## Appendix B

Here we describe how we fitted our 80 measurements of the set $\{N_{IC}, n_{0.5}, T_{low}\}$ using the three step procedure developed by D10 (herein method #2). In the first step, the data were binned into four $(273.16 - T_{low})$ subsets; the number of samples in the four subsets is provided in Table 3. In the second step, values of $ln(p_i)$ and $q_i$ were derived for each subset by regression. Here "$i$" indicates the temperature subset and the form of the fitted equation is

$$ln(N_{IN,i}) = ln(p_i) + q_i \cdot ln(n_{0.5,i}) \quad \text{(B1)}$$

In the third step, the values of $ln(p_i)$ were regressed vs. $ln(273.16 - T_{low,i})$, and also, the values of $q_i$ were regressed vs. $T_{low,i}$. In these regressions the $T_{low,i}$ is the average of the subset. The slopes and intercepts of these regressions define the coefficients $ln(a)$, $b$, $c$ and $d$ for method #2.

$$ln(a) = \text{intercept}\left(ln(p_i)\ vs.\ ln(273.16 - T_{low,i})\right) \quad \text{(B2)}$$

$$b = \text{slope}\left(ln(p_i)\ vs.\ ln(273.16 - T_{low,i})\right) \quad \text{(B3)}$$

$$c = \text{slope}\left(q_i\ vs.\ (273.16 - T_{low,i})\right) \quad \text{(B4)}$$

$$d = \text{intercept}\left(q_i\ vs.\ (273.16 - T_{low,i})\right) \quad \text{(B5)}$$